Equilibrium theory based design space for the MCSGP process

Fabian Steinebach, Martin Krättli, Giuseppe Storti, Massimo Morbidelli*

Institute for Chemical and Bioengineering, Department of Chemistry and Applied Biosciences, ETH Zurich, 8093 Zurich, Switzerland

Manuscript to be submitted to:

* Corresponding author: Prof. Dr. Massimo Morbidelli, ETH Zurich, HCI F-129, Vladimir-Prelog-Weg 1, CH-8093 Zurich, Switzerland. Tel.: +41 44 632 30 34; fax: +41 44 632 10 82.

E-mail address: massimo.morbidelli@chem.ethz.ch (M. Morbidelli).

Highlights

- Constraints under which the twin-column MCSGP process achieves stable operation are described.
- Equations for the elution volume based on equilibrium theory for ion-exchange chromatography for subsequent linear gradients are derived.
- Combining the predicted elution volumes with the constraints result in a design space, similar to the “triangle theory” for SMB.
- Thereby feasible and robust operation points can be obtained with limited experimental effort.

Abstract

A procedure for designing the operation parameter space for the twin-column MCSGP (multi column countercurrent solvent gradient purification) process for the purification of therapeutic proteins is derived. This is based on the equilibrium theory, which assumes instantaneous equilibrium conditions. As the MCSGP process allows protein separation with a linear modifier gradient, all equations are derived in terms of the covered distance as function of the modifier concentration in ion-exchange chromatography. All constraints, which need to be fulfilled in order to obtain a stable process with maximum yield and purity, are described as function of the different process parameters. For operation parameters within the parameter space where all constraints are fulfilled, a stable process is predicted. Additionally, on the boundary of this region, the optimal operation point in terms of buffer consumption and productivity can be found. Besides this, the presented design space can help to analyze the impact of different process parameters on performance and stability and therefore to establish conditions for a robust operation of the process.

1 Introduction

Multi-column chromatography processes are currently considered as one of the major opportunities to reduce costs in the downstream processing of therapeutic proteins [1,2]. In particular, processes for both capture [3,4], especially in the frame of an integrated continuous process [5,6] and polishing steps [7,8] have been investigated. As such processes have a larger number of process steps, and hence more design parameters than single-column processes, the process design is more complicated. Therefore, both model-based [9–12] and experiment-based [13,14] process design approaches have been proposed in order to find optimal operating conditions.

For the SMB (simulated moving bed) process [15,16], which enables in its original four-zone set-up an improved separation of binary mixtures [17], the “triangle theory” [18–20] is often used for process design. With this procedure not only optimal operating conditions, but also different regions of separation regimes can be identified in the mass flow rate ratios parameter space. This approach, which can also be applied to batch processes [21], is based on the equilibrium theory, for which mass transfer and axial dispersion effects are neglected [22].

Since the SMB process is limited to binary separations with constant modifier concentration, the MCSGP (multi-column continuous countercurrent purification) process was developed [23,24], enabling ternary separation with a linear modifier gradient as well as the subsequent operations needed for the regeneration of the stationary phase. In this process, the overlapping regions of the chromatogram are recycled, while pure fractions are collected, so that a high yield and purity can be achieved. Implementations include six [25], three [26] and most recently two [7,14,27] column processes.

The goal of this work is the development of a design procedure, similar to the “triangle theory”, for the twin-column MCSGP process. As the adsorption behavior depends on the modifier concentration, the equilibrium theory needs to account for the linear gradient elution [28] as well as steps in the modifier profile [29,30]. Here the case of ion-exchange chromatography with a linear isotherm, described by the stoichiometric displacement model [31,32], is considered. Therefore in section 2 the process is characterized and constraints for robust operation are formulated, while in section 3 the necessary equations are derived. When combining these two parts, results about the process stability and performance are obtained.

2 The twin-column MCSGP process

2.1 Process description

A detailed process description can be found in previous publications [7,14,27]. In short, this two column cyclic process, for which the flow scheme is shown in Figure 1, with reference

to the chromatogram represented in the sides of the same figure, is operated by alternating between interconnected steps (grey background) when recycling overlapping regions of the chromatogram, and batch steps, when loading feed F, eluting the impurities W (weak adsorbing) and S (strong adsorbing) or the product P. During the interconnected steps (I1 and I2) the outlet stream of column position 1 is mixed with an effluent stream E in order to achieve re-adsorption conditions on column position 2. After these four steps, the two columns switch their position and the same tasks are repeated. By recycling the overlapping regions of the chromatogram and eluting the pure product fraction, both a high purity and yield can be achieved.

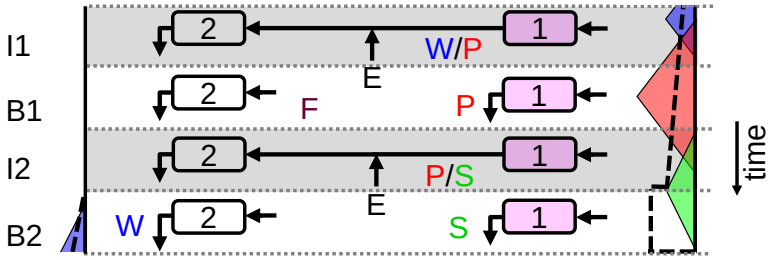

Figure 1: Flow scheme of half a cycle of a twin-column MCSGP process with time increasing from top to bottom. The schematic chromatograms are shown next to each column.

2.2 Process design

The process itself has various degrees of freedom, for which operation parameters need to be defined. The process is constituted by a sequence of steps, which are shown in Figure 2 for a single column, where again interconnected phases are highlighted in grey. We define the length of each step j by a dimensionless elution volume θ_j that is defined as the applied buffer volume divided by the void volume.

$$\theta_j = \frac{V_j}{V_{void}} \tag{1}$$

As during the interconnected phases liquid is transferred from one column to the other (I1 and I2 in Figure 1), it makes sense to couple the corresponding flow rates by defining fixed

recycle ratios (RR_j) between the streams as $\theta_{E,I1} = \theta_{I11}/RR_{I1}$ and $\theta_{E,I2} = \theta_{I21}/RR_{I2}$ where $\theta_{E,I1}$ and $\theta_{E,I2}$ and are the corresponding compensation volumes, that is the volume added in the mixing node in between the two columns. Similarly, the feed θ_{B12} and product volumes θ_{B11}can be coupled by defining a fixed feeding ratio FR and hence $\theta_{B12} = FR\ \theta_{B11}$. This is favorable as both steps are performed in parallel during B1, and thereby a larger load amount results in a larger product fraction. Additionally during the step B2 the corresponding volumes for W elution θ_{B22} and the CIP (cleaning-in-place) step θ_{B21} need to be defined.

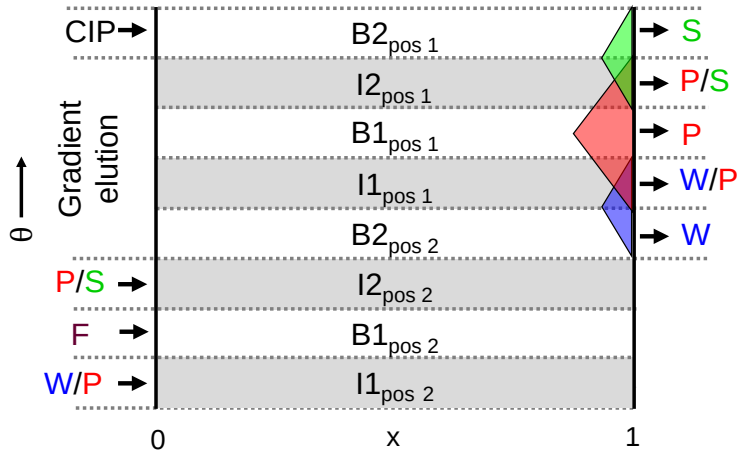

Figure 2: Inlet (left side) and outlet streams (right side) for one column over one cycle of the twin-column MCSGP process. Volume, equivalent to time, increases from bottom to top.

Besides the volumes, also the modifier concentration needs to be defined. This can be done by introducing a linear gradient which is eluting the different components, as schematically shown in Figure 1 (dotted line). The resulting modifier concentration in column position 2 during the interconnected phases can then be calculated from the modifier concentration in the compensation flows $c_{mod,E}$.

2.3 Constraints for robust performance

As in this process both columns perform the same operation, shifted by half a cycle, it is worth to consider the length-volume plane of a single column and follow its inlet and outlet streams over one cycle. Of course the established representation is repeated under cyclic steady

state conditions. Once more, this is schematically shown in Figure 2. Starting with an empty column at column position 2, loading is performed during the three steps $I1_2$, $B1_2$ and $B2_2$. Afterwards the gradient elution is started, with the subsequent elution of W, the overlapping region P/S, pure product P, the overlapping region P/S and finally S during the CIP step.

In order to operate the process in a stable manner with high purity and yield, different constraints need to be fulfilled. Similar considerations have been reported previously for a 5-column MCSGP process [33]. In the following, these constraints are expressed for the covered distance Δx of the characteristic curves, where $x = z/L_{column}$ is the dimensionless position, normalized between 0 for the column inlet and 1 for the column outlet as shown in Figure 2. As characteristic curves for the same component cannot intersect with each other [22], the characteristic curve describing the first (last) elution will be the one entering the column first (last). For the same reason the constraints can be limited to the first (last) characteristic curves. These constraints can also be expressed for the elution volumes and corresponding inequalities for the volumes are given in the supplementary information.

For the target Protein P, the earliest elution is allowed to occur during $I1_1$, as previous elution will result in a decreased yield. As the corresponding first characteristic curve starts at the beginning of $I1_2$, this constraint can be expressed by the sum of covered distances during the intermediary phases

$$0 + \Delta x_{P,I12} + \Delta x_{P,B12} + \Delta x_{P,I22} + \Delta x_{P,B22} < 1 \tag{2}$$

Similarly, the last product, which enters the column at the end of $I2_2$, is not allowed to elute after $I2_1$, as it is otherwise lost in the CIP step and therefore

$$0 + \Delta x_{P,B22} + \Delta x_{P,I11} + \Delta x_{P,B11} + \Delta x_{P,I21} > 1 \tag{3}$$

Regarding P, two more constraints need to be defined. As in steady-state operation the same amount of product needs to be collected than it is loaded, the characteristic curves

evolving from the first and last point of the loading phase $B1_2$ need to leave the column during $B1_1$, knowing that mass transfer limitation will result in a broader peak.

$$0 + \Delta x_{P,B12} + \Delta x_{P,I22} + \Delta x_{P,B22} + \Delta x_{P,I11} < 1 \tag{4}$$

$$0 + \Delta x_{P,I22} + \Delta x_{P,B22} + \Delta x_{P,I11} + \Delta x_{P,B11} > 1 \tag{5}$$

Additionally, two constraints for each impurity need to be defined. For the weak adsorbing impurity, accumulation in the I1 phase is avoided and hence cyclic steady state is achieved when some W elutes during the $B2_2$ phase

$$0 + \Delta x_{W,I12} + \Delta x_{W,B12} + \Delta x_{W,I22} + \Delta x_{W,B22} > 1 \tag{6}$$

Product contamination is avoided when the last W entering the column is eluted before product collection occurs.

$$0 + \Delta x_{W,I22} + \Delta x_{W,B22} + \Delta x_{W,I11} > 1 \tag{7}$$

Similarly, for the strong adsorbing impurity S the following constraints can be formulated, where accumulation during the I2 phase is avoided by some S eluting after this phase

$$0 + \Delta x_{S,B12} + \Delta x_{S,I22} + \Delta x_{S,B22} + \Delta x_{S,I11} + \Delta x_{S,B11} < 1 \tag{8}$$

In a last constraint, product contamination is avoided when the earliest elution of S occurs after the product collection

$$0 + \Delta x_{S,B22} + \Delta x_{S,I11} + \Delta x_{S,B11} + \Delta x_{S,I21} < 1 \tag{9}$$

It is worth noting that the inequalities (2) and (3) guarantee a theoretical yield of 100%, while eq. (7) and (9) guarantee a theoretical purity of 100%, without the need of base-line separation. We refer to these performances since they hold true in the limit of equilibrium theory, which implies that equilibrium conditions apply at any time and location, with no effect of any dispersive process.

As in practical applications several impurities are often involved, key components, which have the closest adsorption behavior to P, need to be selected. It follows that, for all other impurities, accumulation and product contamination are avoided.

3 Equilibrium theory for step-wise linear gradients

3.1 Column mass balance

Under the assumptions of no axial dispersion and instantaneous equilibrium between the solid phase concentration q_i and the liquid phase concentration c_i, the mass balance for component i can be written as

$$\frac{1}{A}\frac{\partial c_i}{\partial z} + \varepsilon\frac{\partial c_i}{\partial V} + (1-\varepsilon)\frac{\partial \mathrm{q}_i}{\partial V} = 0 \tag{10}$$

where A is the cross-section area, V the solvent volume and ε the porosity, which is here assumed to be the same for all components. Here we consider the case of a linear isotherm

$$q_i = H_i c_i \tag{11}$$

where H_i is the Henry constant, which in ion-exchange chromatography depends on the modifier concentration c_{mod} according to

$$H_i = \alpha_i (c_{mod})^{z_i} \tag{12}$$

and α_i and z_i are component specific constants.

Introducing the phase ratio $\nu = (1-\varepsilon)/\varepsilon$ and the dimensionless paremeters $x = z/L_{column}$ and $= V/V_{void}$, where $V_{void} = L_{column}A\varepsilon$ results in the following equation

$$\frac{\partial c_i}{\partial x} + (1+\nu H_i)\frac{\partial c_i}{\partial \theta} = -c_i\nu\,\frac{\partial H_i}{\partial \theta} \tag{13}$$

which can be transformed with the method of characteristics into a system of ordinary differential equations [22]

$$\begin{cases} \frac{d\theta}{dx} = 1 + \nu H_i \\ \frac{dc_i}{dx} = -c_i\nu\,\frac{\partial H_i}{\partial \theta} \end{cases} \tag{14}$$

The movement of a component along a characteristic curve is described by the first of equations (14), while the second describes the concentration change along this curve.

3.2 Modifier profile

Here we consider the case of linear gradients for the modifier profile. The corresponding boundary condition, given by the inlet modifier profile c_{mod}^{i}, can be expressed with the gradient start concentration c_0 and slope m as $c_{mod}^{i}(V) = c_0 + mV$, which results in a position and volume dependent modifier concentration

$$c_{mod}(x, \theta) = c_0 + mV_{void}(\theta - x) \tag{15}$$

In the dimensionless length-volume plane, these trajectories have a slope of unity and identify a constant concentration value.

3.3 Results for biomolecules

3.3.1 Movement of biomolecules along the column

A solution for eq. (14) for the protein profile can be obtained after plugging in eq. (15) and (12) and defining a new parameter $\varphi = \theta - x$, which is the dimensionless buffer volume at the column inlet of the corresponding modifier trajectory. As boundary conditions, the start (x_k, θ_k) and end positions (x_{k+1}, θ_{k+1}) are defined. Separation of variables and integration, as shown in the supplementary information, results in

$$\frac{(c_0+mV_{void}\varphi_{k+1})^{1-z_i}}{\nu\,\alpha_i(1-z_i)mV_{void}} - \frac{(c_0+mV_{void}\varphi_k)^{1-z_i}}{\nu\,\alpha_i(1-z_i)mV_{void}} = (x_{k+1} - x_k) \tag{16}$$

Which allows computing the covered distance $(x_{k+1} - x_k) = \Delta x_k$ in an interval defined by φ_k and φ_{k+16}, based on the adsorption behavior, defined by α_i and z_i, and the gradient parameters k and mV_{void}. Therefore the brackets in the numerators on the left side of eq. (16) represent the corresponding modifier concentration.

An illustrative example is shown in the upper segment of Figure 3, where the domain of influence of the corresponding gradient segment is defined by the slope of the characteristic curve of the modifier. As the constraints expressed in section 2.3 are formulated with respect to the outlet position, the corresponding buffer concentration needs to be calculated from $\varphi_{k+1} = \theta_{k+1} - 1$.

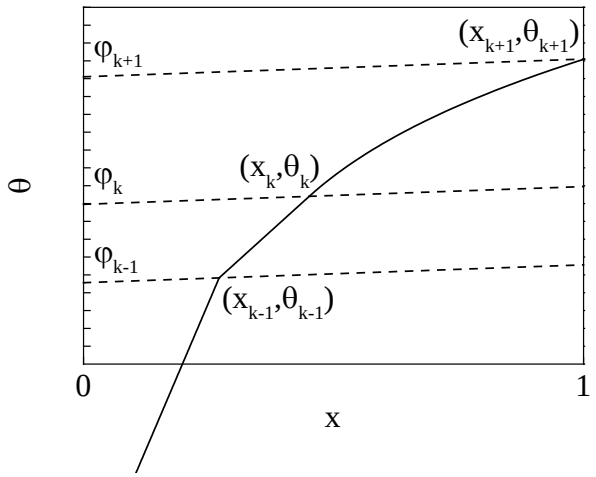

Figure 3: Dimensionless length-volume plane with a trajectory, representing the movement in a column during a step-wise linear gradient. Dotted lines represent modifier trajectories and the solid line the trajectory of a protein.

In case of a step in the modifier concentration, which is mathematically defined as $m = \infty$, there is no change in the position as

$$\lim_{m^i \to \infty} \Delta x(m) = 0 \tag{17}$$

This case is shown at the point (x_{k-1}, θ_{k-1}) in Figure 3. In the opposite case, where a constant modifier concentration is applied and hence $m = 0$ it follows

$$\lim_{m \to 0} \Delta x(m) = \frac{\varphi_{k+1} - \varphi_k}{\nu\, \alpha_i k^{z_i}} \tag{18}$$

which can be rearranged to obtain the well-known expression for isocratic elution $V = V_{void}(1 + \nu \alpha_i {c_{mod}}^{z_i})$. This constant movement is shown by the segment from φ_{k-1} to φ_k in Figure 3.

It is worth noting that eq. (16) can also be rearranged to calculate the dimensionless elution volume, where at the column outlet $x_{k+1} = 1$, as

$$\theta_{k+1} = x_{k+1} + \frac{\left[\nu\alpha_i(1-z_i)mV_{void}(x_{k+1}-x_k)+\left(k+mV_{void}(\theta_k-x_k)\right)^{1-z_i}\right]^{\frac{1}{1-z_i}}-k}{mV_{void}} \tag{19}$$

and similar expressions have been obtained previously by Stahlberg [34] and Jandera [35].

3.3.2 Protein concentration along a characteristic curve

The solution of the second of equations (14) describes the concentration change along a characteristic curve as

$$\frac{c_{i,A}}{c_{i,B}} = \left(\frac{c_{mod}(B)}{c_{mod}(A)}\right)^{z_i} \tag{20}$$

where A and B are two points on a characteristic curve. This result can be derived from the fact, that independent of the isotherm shape, the solid phase concentration q_i remains constant along a characteristic curve [29,30]. This results in a concentration increase under modifier gradient elution.

3.4 Mass balances for mixing nodes

For the interconnected phases the modifier gradient after the mixing with the compensation buffer needs to be calculated. Here the gradient elution, which starts in the $B2_2$ phase and ends after the $I2_1$ phase is internally recycled after mixing with the isocratic compensation streams during the interconnected phases I1 and I2. Hence the resulting gradient in phase $I1_2$ can be described with the parameters

$$c_{0,I12} = \frac{c_{mod,E}\,\theta_{E,I1}+\left(c_{0,grad}+m_{grad}V_{void}(\theta_{B22}-1)\right)\theta_{I11}}{\theta_{E,I1}+\theta_{I11}} \tag{21}$$

$$m_{I12} = \frac{m_{grad}\,{\theta_{I11}}^2}{\left(\theta_{E,I1}+\theta_{I11}\right)^2} \tag{22}$$

Similarly, the resulting gradient during phase I2 is defined by the parameters

$$c_{0,I22} = \frac{c_{mod,E}\,\theta_{E,I2}+\left(c_{0,grad}+m_{grad}V_{void}(\theta_{B22}+\theta_{I11}+\theta_{B12}-1)\right)\theta_{I21}}{\theta_{E,I2}+\theta_{I21}} \tag{23}$$

$$m_{I12} = \frac{m_{grad}\,{\theta_{I21}}^2}{\left(\theta_{E,I2}+\theta_{I21}\right)^2} \tag{24}$$

Additionally, the resulting dimensionless volumetric flow rate is given by $\theta_{I12} = \theta_{E,I1} + \theta_{I11}$ and $\theta_{I22} = \theta_{E,I2} + \theta_{I21}$.

4 Materials and methods

4.1 Simulations

In order to validate the model results described above and based on equilibrium theory, a more realistic model was used. Therefore, instead of the instantaneous equilibrium, a lumped mass transfer resistance k_{tot} was introduced as

$$\frac{\partial \mathrm{q}_i}{\partial V} = k_{tot}(H_i c_i - \mathrm{q}_i) \tag{25}$$

This term was introduced in eq. (10). The resulting mass-balance equations were discretized in space and solved with a FORTRAN implemented MUSCL scheme as explained in [10].

4.2 Separation task

With illustrative purposes, the separation of charge isoforms of a monoclonal antibody is considered, for which experimental results are reported in a previous publication [14]. The separation is conducted on a strong cation exchanger (YMC BioPro S10, YMC Europe GmbH, Dinkslaken, Germany) with a 20 mM phosphate Buffer pH 6.1 and a NaCl gradient. Here, from the ionic strength of the Buffers, for the low-salt Buffer a NaCl concentration of 1.45 g/L and for the high salt Buffer a NaCl concentration of 10.16 g/L were calculated. For the preparative separation a linear modifier gradient, whose parameters are reported in Table 1, was used.

Table 1: Operation parameters for the MCSGP process

RR_1, FR, RR_2	2, 5, 0.5
$k_{grad}, m_{grad}, c_{mod,E}$	5.4 mg/mL, 0.0339m g/mL/mL, 1.34g/L

θ_{B21} , θ_{B22}	5, 14.3
feed concentration	c_{mod}= 5 mg/mL c_i= 0.25, 0.5, 0.25 mg/mL (W, P, S)
column size	d_{column}=0.5cm, L_{column}= 19.2 cm (V_{void}=2mL)

The model parameters for this separation task were obtained from analytical injection of the different charge isoforms on a 1mL column on an Agilent 1200 system HPLC (Agilent, Santa Clara, CA, USA) with a flowrate of 1 mL/min. The adsorption isotherm parameters have been determined from linear gradient experiments [36] and the mass transfer coefficient from HETP measurements, as shown in the supplementary information. All estimated values of the model parameters are summarized in Table 2.

Table 2: Values of model parameters for charge isoform separation

Parameter	Value
α_W, α_P, α_S	$10^{6.8}$, $10^{7.16}$, $10^{7.57}$
z_W, z_P, z_S	-7.24, -7.54, -7.91
porosity	0.52
k_{tot}	28.7 min^{-1}
Q	300 cm/h

5 Results and discussion

5.1 Results for batch elution

Figure 4 shows the comparison between the simulation results, including mass-transfer resistance, and the ideal model results for a 15 column volumes load and subsequent linear gradient elution over 15 column volumes. For the ideal model, the elution volume of the front

was calculated from the covered distance during loading, determined with eq. (18), which was then plugged into the expression for gradient elution (eq. (19)). As the last protein enters the column at the end of the loading, the peak rear position was calculated with eq. (19) and the starting position $\theta_k - x_k = 0$. Afterwards eq. (20) was used to calculate the protein concentration in the corresponding segments.

As the ideal model takes only the peak broadening by loading into account, but not the additional peak broadening due to mass transfer, the ideal peaks are sharper. From eq. (18) and (19) it can be seen that longer loading at high modifier concentration increase the final peak broadness, while steep gradients compress the peak. Regarding the peak position, a good agreement between the two models is observed.

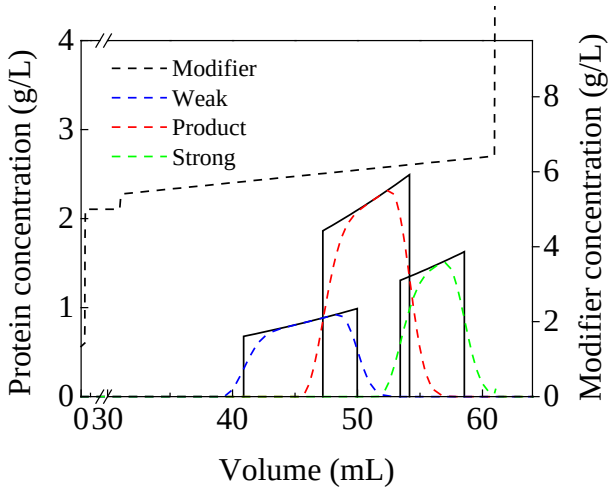

Figure 4: Comparison of the simulation results including mass transfer limitations (dotted lines) and the equilibrium-theory results for batch elution (solid lines). Q=300 cm/h, column length=10 cm, column volume =2 mL.

5.2 Design space in the θ-plane

In general the analysis for stable operation is performed by testing different combinations of operation parameters fulfilling the constraints listed in section 2.3. As these constraints only consider the peak position, but not the concentrations, the following consideration is based on

eq. (16) for the gradient phases and eq. (18) for the feeding during θ_{B12}. The calculated covered distances Δx were then entered into the constraints from eq. (2) to (9).

As shown in section 2.2, the eight different volumes and corresponding modifier concentrations result in numerous possible combinations, each one describing a unique set of process parameters. Here the complexity can be reduced by implementing constant recycle and feed ratios, which is also done in practice [14]. Additionally, the CIP step has no impact on the separation performance; therefore it is not part of the formulated constraints and can be kept constant. All fixed values were already listed in Table 1. Since the modifier gradient slope is kept constant [7], the consideration is limited to the four volumes θ_{B22}, θ_{I11}, θ_{B11} and θ_{I21}. Similar to the triangle theory for SMB, where the consideration is limited to the intermediate separation region, the parameter θ_{B22} can be fixed to fulfill the constraints expressed in eq. (2) and (6). Similarly, the sum of the volumes, which defines the gradient end-point, can be fixed in order to fulfill eq. (3) and (8). Here 14.3 was chosen for θ_{B22} and 6.1 for the sum of θ_{I11}, θ_{B11} and θ_{I21} with the recycle ratios given in Table 1. The corresponding representation is shown in the supplementary information.

Fixing these values results in two more degrees of freedom, which describe the start- and endpoint of the θ_{B11} phase, during which product is collected. Regarding the product purity and process performance, these boundaries are most critical. From the previously fixed values it follows that also the length of the recycle ratios θ_{I11} and θ_{I21} is given. The resulting design space, which is a slice of constant volume through a three-dimensional design space with θ_{I11}, $\theta_{B11}$and θ_{I21} on each axis, is a triangle with equal edge length. This is shown in Figure 5, where every point in this triangle represents a unique set of values for the θ_{I11} , θ_{B11} and θ_{I21} parameters. For example, in each corner of the triangle, only the corresponding task is performed, while in the center point all tasks are performed with the same buffer volume. In order to find suitable operation conditions, the constraints in section 2.3 were evaluated for all

possible combinations. The region in which all constraints are fulfilled and hence a cyclic steady state with complete separation is predicted, as well as the neighboring regions, in which one constraint is violated, are shown in Figure 5.

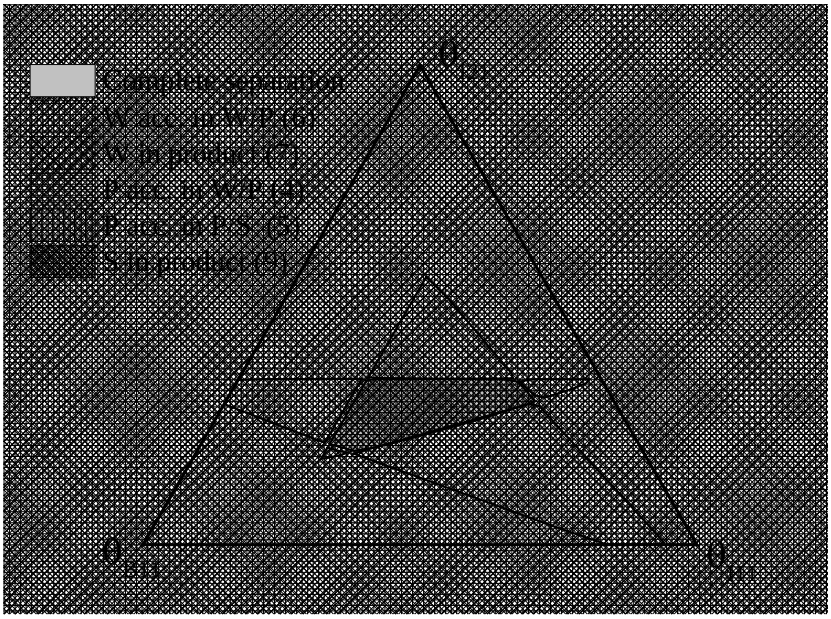

Figure 5: Design space for a twin-column MCSGP process including neighboring regions with corresponding violated constraints. Numbers in the legend refer to the corresponding constraints in section 2.3. Outside of the described areas two or more constraints are violated.

It can be seen that for large θ_{B11} values, which represent operation points with a broad product collection window, the feasible operation range is limited by the constraints formulated in eq. (7) and (9), as in this case impurities are collected together with P, reducing the product purity. On the other side, small values for θ_{B11} , which is equivalent to a small loading amount, results in a violation of eq. (6). In this case the first W elutes too late, resulting in an accumulation of this impurity in the W/P recycle stream and therefore in an accumulation in the system. In the frame of the equilibrium theory, such accumulation is growing indefinitely without affecting purity and yield. However, it is clear that this accumulation does not result in a cyclic steady-state and will instead in reality ultimately lead to a decreased performance. Therefore such operation points are not feasible and excluded by the corresponding constraint.

In the case of a long θ_{I11} phase, accumulation of P in the corresponding interconnected phase occurs, as too much product is eluting prior to the product collection and the corresponding constraint expressed in eq. (4) is violated. In the opposite case, a too long θ_{I21} recycle phase results in product accumulation during this phase and a violation of eq. (5). Also in this case, these accumulation effects do not lead to a decreased performance in terms purity. However, as discussed previously for the W accumulation, also P accumulation will grow indefinitely and cyclic steady state is not possible. Again in reality, non-linear effects will result in a shift of the peak position and therefore lower the performance. Additionally for these operating points the product will exhibit an increasing residence time, as a higher fraction is recycled. Hence these operating points are not feasible and excluded.

5.3 Process performance and optimal operation

The different θ_j values discussed in the previous section affect not only purity and yield, but also the process performance in terms of cyclic productivity and buffer consumption. The amount of feed purified per cycle increases linearly with the θ_{B11} value, as load amount in phase θ_{B12} and θ_{B11} are coupled with a fixed feed ratio. Therefore parallel lines of constant cyclic productivity can be included in the design space, with productivity increasing towards the bottom left corner. This is shown by the dotted line in Figure 6, where the reported numbers represent the feed amount in terms of the dimensionless feed volume θ_{B12}.

Additionally, the total amount of buffer per amount of purified product can be calculated. Solid lines representing of constant buffer consumption are included in Figure 6. In general, less recycling decreases the buffer consumption, and hence this value decreases towards the θ_{B12} corner. As different recycle ratios for the different interconnected states are applied, these lines are not parallel. The reported numbers represent express the buffer consumption per amount as feed volume, as calculated in the supplementary information.

Combining the results for productivity and buffer consumption leads to the conclusion that optimal performance is achieved in the bottom left corner of the stable operation region. As shown in Figure 5, this is in fact the point where product collection goes from the end of W elution up to the first S elution and therefore θ_{B11} is at its largest value. It has to be noted that as this optimal operation point is on the boundary of the stable operation region, small changes in the process parameters or elution behavior will have a large impact on the product purity. Hence when choosing an operation point, a trade-off between performance and stability needs to be considered and more stable operation points can be identified by moving towards the center of the stable operation region.

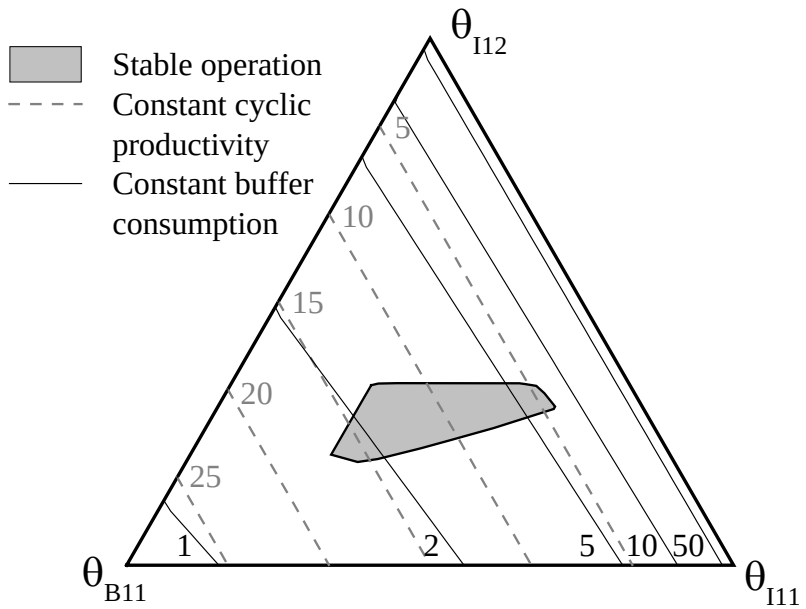

Figure 6: Design space for a twin-column MCSGP process including lines for constant cyclic productivity and buffer consumption.

Finally, it is worth noting that the constant ratio between feed and product volume results in a constant product concentration for all points of the design space, where the product concentration is increased by the factor FR.

5.4 Impact of operation parameters and safety margin

The design space derived in section 5.2 can be used to analyze the impact of different perturbations or changes in buffer composition or process parameters on the process stability. Here as an example the modifier concentration in the feed was varied. As shown in Figure 7A, a small increase from the base-case of 5 g/L to 5.1 g/L has a large impact on the size of the stable operation region. Under this perturbation, the previously optimal operation point is outside of the region of complete separation, as the constraints for product purity is not fulfilled with the corresponding set of operation parameters. However operation points with a smaller load amount are still able to fulfill all constraints.

On the other hand, in Figure 7A the feasible region for a feed modifier concentration of 4.5 g/L is shown. In this case the loading amount can be increased without violating the constraints, which allows operating the process with better performance. It is remarkable that these important and not straightforward results can be very easily obtained from the knowledge of the design space provided by the equilibrium theory approach developed above.

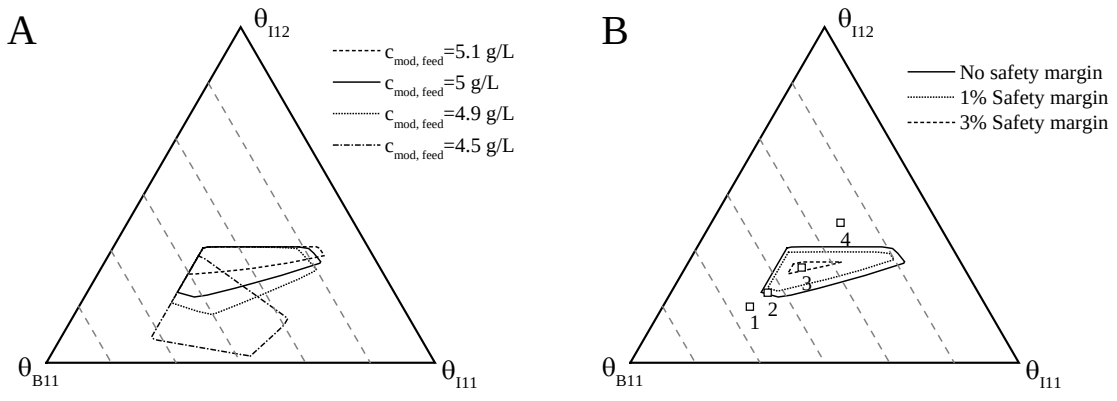

Figure 7A: Design space for different modifier concentrations in the feed. B: Design space with different safety margins as well as the four different operation points discussed in the text.

In Figure 7B the same design space with different safety margins is shown. As the consideration is based on the ideal model in the linear range of the isotherm, additional peak broadening will occur in practical implementations. This can be taken into account by

multiplying the dimensionless column length in the constraints (2) to (9) by a suitable safety factor. This corresponds to impose the corresponding inequality to be fulfilled a few percent before or after the actual column length. Therefore the feasible operation range decreases in size, showing that central operation points are indeed the most robust ones. Hence for such operation points the decreased purity and yield due to mass-transfer resistance and axial dispersion should be limited.

5.5 Comparison to model simulation results

In order to quantitatively support the above conclusion, the MCSGP process was simulated with the model presented in 4.1 for the four different operation points shown in Figure 7B. For point 1 the purity constraints are violated, as it can be seen from Figure 5. Indeed, numerical simulations resulted in a purity of 88% and a yield of 99.7%, where both impurities partially elute during product collection. Point 2, which is at the boundary of optimal operation, resulted in a purity of 94% and a yield of 99.7%. The deviation from the predicted purity of 100% comes from mass transfer limitations broadening the peaks and hence decreasing the purity. For Point 3, which is more towards the center of the stable operation region, a purity of 98% and a yield of 99.9% were obtained. One can therefore conclude that the safety margin introduced in Figure 7B is in this case large enough to adjust for broader peaks due to non-ideality effects. For point 4, which is outside of the design space and instead in the region of P accumulation, as predicted no stable operation was achieved due to product accumulation, which prevents a cyclic steady state to be reached. This combination of operation parameters did not allow reaching a cyclic steady-state within 15 cycles. In contrast, for all the other operation points a cyclic steady state was achieved within 3 cycles.

6 Conclusion

The developed procedure, based on equilibrium theory, allows computing the design operating parameter space for efficient and robust operation of the twin-column MCSGP

process for a given separation task. For combinations of operation parameters within such parameter space, stable operation is predicted and proven with simulation results. The boundaries of this region are expressed in terms of the covered distance, as this value can easily be calculated with equations derived from the column mass balance using equilibrium theory. The additional peak broadening by mass-transfer limitations can be accounted through a proper safety margin.

As the underlying equilibrium theory takes peak broadening by loading, including recycle and feed streams, into account, the effect of different parameters on the process performance and stability can be analyzed. It is worth mentioning that the developed procedure has a strong general character. In particular, also for batch processes with linear gradient elution, the effect of loading on the peak broadness can be analyzed with the presented equations. In addition, by adjusting the constraints, this procedure can be extended to other multi-column chromatographic processes, while it can also be extended to other types of chromatography by introducing proper equilibrium isotherms, such as reversed-phase or hydrophobic interaction applications.

Finally, it should be noted that the developed design space allows designing not only stable and efficient, but also robust processes, where small perturbations, such as changes in the modifier feed concentration, do not affect significantly the process purity and yield. With the identified optimal operation point and additional control loops, which adjust the product elution, optimal operation even under perturbations can be achieved.

Acknowledgement

We would like to acknowledge Daniel Baur for implementing the FORTRAN code.

Nomenclature

α_i	Component-specific pre-factor for Henry constant
ε	Porosity (-)
$\varphi = \theta - x$	Position-normalized dimensionless volume (-)
$\theta = V/V_{void}$	Dimensionless volume (-)
$\nu = (1-\varepsilon)/\varepsilon$	Phase ratio (-)
A	Column cross-section area (cm^2)
c_i	Liquid phase concentration of component i (mg/ mL)
c_{mod}	Modifier concentration (mg/ mL)
d_{column}	Column diamter (cm)
FR	Feed ratio
H_i	Henry constant for component i (-)
k	Gradient start concentration (mg/mL)
k_{tot}	Lumped mass-transfer coefficient min^{-1}
L_{column}	Column length (cm)
m	Gradient slope (mg/ mL/ mL)
Q	Superficial velocity (cm/h)
q_i	Solid phase concentration of component i (mg/ mL)
RR_j	recycle ratio during interconnected phase j
V	Buffer volume (mL)
$V_{void} = L_{column}A\varepsilon$	Void volume (-)
$x = z/L_{column}$	Dimensionless position along the column (-)
z	Position along the column (cm)
z_i	Effective charge of component i (-)

References

[1] F. Steinebach, T. Müller-Späth, M. Morbidelli, Continuous counter-current chromatography for capture and polishing steps in biopharmaceutical production, Biotechnol. J. 11 (2016) 1126–1141. doi:10.1002/biot.201500354.

[2] A. Jungbauer, Continuous downstream processing of biopharmaceuticals., Trends Biotechnol. 31 (2013) 479–92. doi:10.1016/j.tibtech.2013.05.011.

[3] F. Steinebach, M. Angarita, D.J. Karst, T. Müller-Späth, M. Morbidelli, Model based adaptive control of a continuous capture process for monoclonal antibodies production, J. Chromatogr. A. 1444 (2016) 50–56. doi:10.1016/j.chroma.2016.03.014.

[4] E. Mahajan, A. George, B. Wolk, Improving affinity chromatography resin efficiency using semi-continuous chromatography., J. Chromatogr. A. 1227 (2012) 154–62. doi:10.1016/j.chroma.2011.12.106.

[5] V. Warikoo, R. Godawat, K. Brower, S. Jain, D. Cummings, E. Simons, et al., Integrated continuous production of recombinant therapeutic proteins., Biotechnol. Bioeng. 109 (2012) 3018–29. doi:10.1002/bit.24584.

[6] D.J. Karst, F. Steinebach, M. Soos, M. Morbidelli, Process performance and product quality in an integrated continuous antibody production process, Biotechnol. Bioeng. 9999 (2016) 1–10. doi:10.1002/bit.26069.

[7] M. Krättli, F. Steinebach, M. Morbidelli, Online control of the twin-column countercurrent solvent gradient process for biochromatography., J. Chromatogr. A. 1293 (2013) 51–9. doi:10.1016/j.chroma.2013.03.069.

[8] R.-M. Nicoud, The Amazing Ability of Continuous Chromatography To Adapt to a Moving Environment, Ind. Eng. Chem. Res. 53 (2014) 3755–3765. doi:10.1021/ie5005866.

[9] F. Steinebach, M. Angarita, D.J. Karst, T. Müller-späth, M. Morbidelli, Model based adaptive control of a continuous capture process for mAb production, J. Chromatogr. A. (2016).

[10] D. Baur, M. Angarita, T. Müller-Späth, M. Morbidelli, Optimal model-based design of the twin-column CaptureSMB process improves capacity utilization and productivity in protein A affinity capture, Biotechnol. J. (2015). doi:10.1002/biot.201500223.

[11] C.K.S. Ng, H. Osuna-Sanchez, E. Valéry, E. Sørensen, D.G. Bracewell, Design of high productivity antibody capture by protein A chromatography using an integrated experimental and modeling approach., J. Chromatogr. B. Analyt. Technol. Biomed. Life Sci. 899 (2012) 116–26. doi:10.1016/j.jchromb.2012.05.010.

[12] N. Andersson, H.-K. Knutson, M. Max-Hansen, N. Borg, B. Nilsson, Model-Based Comparison of Batch and Continuous Preparative Chromatography in the Separation of Rare Earth Elements, Ind. Eng. Chem. Res. 53 (2014) 16485–16493. doi:10.1021/ie5023223.

[13] O. Kaltenbrunner, L. Diaz, A. Hu, M. Shearer, Continuous bind-and-elute protein a capture chromatography: Optimization under process scale column constraints and comparison to batch operation, Biotechnol. Prog. (2016). doi:10.1002/btpr.2291.

[14] F. Steinebach, N. Ulmer, L. Decker, L. Aumann, M. Morbidelli, Empirical design of a twin-column MCSGP process, submitted (2016).

[15] A. Rajendran, G. Paredes, M. Mazzotti, Simulated moving bed chromatography for the

separation of enantiomers., J. Chromatogr. A. 1216 (2009) 709–38. doi:10.1016/j.chroma.2008.10.075.

[16] R.-M. Nicoud, Chromatographic Processes Modeling, Simulation and Design, Cambridge University Press, Cambridge, 2015.

[17] D.B. Broughton, C.G. Gerhold, Continuous sorption process employing fixed bed of sorbent and moving inlets and outlets, US66079057A, 1961.

[18] M. Mazzotti, G. Storti, M. Morbidelli, Optimal operation of simulated moving bed units for nonlinear chromatographic separations, J. Chromatogr. A. 769 (1997) 3–24.

[19] G. Storti, R. Baciocchi, M. Mazzotti, M. Morbidelli, Design of Optimal Operating Conditions of Simulated Moving Bed Adsorptive Separation Units, (1995) 288–301.

[20] M. Mazzotti, G. Storti, M. Morbidelli, Robust design of countercurrent adsorption separation processes: 2. Multicomponent systems, AIChE J. 40 (1994) 1825–1842. doi:10.1002/aic.690401107.

[21] J. Siitonen, T. Sainio, Unified design of chromatographic separation processes, Chem. Eng. Sci. 122 (2015) 436–451. doi:10.1016/j.ces.2014.10.004.

[22] A. Varma, M. Morbidelli, Mathematical methods in chemical engineering, Oxford University Press, New York, 1997.

[23] G. Strohlein, L. Aumann, M. Mazzotti, M. Morbidelli, A continuous, counter-current multi-column chromatographic process incorporating modifier gradients for ternary separations, J. Chromatogr. A. 1126 (2006) 338–346. doi:DOI 10.1016/j.chroma.2006.05.011.

[24] L. Aumann, M. Morbidelli, A continuous multicolumn countercurrent solvent gradient purification (MCSGP) process., Biotechnol. Bioeng. 98 (2007) 1043–55. doi:10.1002/bit.21527.

[25] L. Aumann, G. Stroehlein, M. Morbidelli, Parametric study of a 6-column countercurrent solvent gradient purification (MCSGP) unit, Biotechnol. Bioeng. 98 (2007) 1029–1042. doi:Doi 10.1002/Bit.21529.

[26] L. Aumann, M. Morbidelli, A semicontinuous 3-column Countercurrent Solvent Gradient Purification (MCSGP) process, Biotechnol. Bioeng. 99 (2008) 728–733. doi:10.1002/bit.21585.

[27] M.M. Papathanasiou, S. Avraamidou, R. Oberdieck, A. Mantalaris, F. Steinebach, M. Morbidelli, et al., Advanced control strategies for the multicolumn countercurrent solvent gradient purification process, AIChE J. 62 (2016) 2341–2357. doi:10.1002/aic.15203.

[28] B. Drake, CONTRIBUTIONS TO THE THEORY OF GRADIENT ELUTION ANALYSIS, Ark. För Kemi. 8 (1955) 1–21.

[29] W. Hao, X. Zhang, K. Hou, Analytical solutions of the ideal model for gradient liquid chromatography., Anal. Chem. 78 (2006) 7828–40. doi:10.1021/ac061318y.

[30] W. Hao, X. Zhang, F. Hu, Analysis of the ideal model for a single component in preparative gradient elution chromatography, Anal. Chem. 79 (2007) 2507–2517. doi:10.1021/ac062006y.

[31] N.K. Boardman, S.M. Partridge, Separation of neutral proteins on ion-exchange resins, Biochem. J. 59 (1955).

[32] W. Kopaciewicz, M.A. Rounds, J. Fausnaugh, F.E. Regnier, Retention model for high-

performance ion-exchange chromatography, J. Chromatogr. A. 266 (1983) 3–21. doi:10.1016/S0021-9673(01)90875-1.

[33] G. Stroehlein, L. Aumann, M. Mazzotti, M. Morbidelli, A continuous, counter-current multi-column chromatographic process incorporating modifier gradients for ternary separations., J. Chromatogr. A. 1126 (2006) 338–46. doi:10.1016/j.chroma.2006.05.011.

[34] J. Ståhlberg, The thermodynamic limit of linear gradient chromatography., J. Chromatogr. A. 1217 (2010) 3172–9. doi:10.1016/j.chroma.2010.02.035.

[35] P. (Pavel) Jandera, J. Churáček, Gradient elution in column liquid chromatography : theory and practice, Elsevier, 1985.

[36] F. Steinebach, R. Wälchli, D. Pfister, M. Morbidelli, Adsorption Behavior of Charge Isoforms of Monoclonal Antibodies on Strong Cation Exchangers, Under Prep. (2016).